AMERICAN SOCIETY of
GENE & CELL
THERAPY

Pre-clinical Safety and Off-Target Studies to Support Translation of AAV-Mediated RNAi Therapy for FSHD

Lindsay M. Wallace,[1] Nizar Y. Saad,[1] Nettie K. Pyne,[1] Allison M. Fowler,[1] Jocelyn O. Eidahl,[1] Jacqueline S. Domire,[1,5] Danielle A. Griffin,[1] Adam C. Herman,[4] Zarife Sahenk,[1,2,3] Louise R. Rodino-Klapac,[1,2] and Scott Q. Harper[1,2]

[1]Center for Gene Therapy, The Research Institute at Nationwide Children's Hospital, Columbus, OH, USA; [2]Department of Pediatrics, The Ohio State University College of Medicine, Columbus, OH, USA; [3]Department of Neurology, The Ohio State University College of Medicine, Columbus, OH, USA; [4]Research Information Solutions and Innovation Infrastructure, The Research Institute at Nationwide Children's Hospital, Columbus, OH, USA

RNAi emerged as a prospective molecular therapy nearly 15 years ago. Since then, two major RNAi platforms have been under development: oligonucleotides and gene therapy. Oligonucleotide-based approaches have seen more advancement, with some promising therapies that may soon reach market. In contrast, vector-based approaches for RNAi therapy have remained largely in the pre-clinical realm, with limited clinical safety and efficacy data to date. We are developing a gene therapy approach to treat the autosomal-dominant disorder facioscapulohumeral muscular dystrophy. Our strategy involves silencing the myotoxic gene *DUX4* using adeno-associated viral vectors to deliver targeted microRNA expression cassettes (miDUX4s). We previously demonstrated proof of concept for this approach in mice, and we are now taking additional steps here to assess safety issues related to miDUX4 overexpression and sequence-specific off-target silencing. In this study, we describe improvements in vector design and expansion of our miDUX4 sequence repertoire and report differential toxicity elicited by two miDUX4 sequences, of which one was toxic and the other was not. This study provides important data to help advance our goal of translating RNAi gene therapy for facioscapulohumeral muscular dystrophy.

INTRODUCTION

Facioscapulohumeral muscular dystrophy (FSHD) is an autosomal-dominant genetic condition with an estimated incidence of 1 in 8,333 to 1 in 20,000 people.[1–5] FSHD was initially classified on the basis of a general pattern of wasting and weakness in muscles of the face, shoulder-girdle, and arms. However, it is now clear that the classical picture of muscle involvement in FSHD is not universal, as some patients may have only limited muscle pathology, whereas others can develop asymmetrical or bilateral weakness in lower limbs, abdominal muscles, and the diaphragm.[6,7] Likewise, there is variability in age at onset, rate of progression, and severity of weakness among individuals within the FSHD community. As a result, some patients may maintain lifelong ambulation, whereas others require wheelchair and caregiver assistance.[7]

In addition to this complicated clinical picture, the molecular mechanisms underlying FSHD are also complex and required decades of investigation to decipher. Great gains in knowledge were achieved in the past decade especially, and the field has focused largely on a model in which de-repression of the *DUX4* gene is a primary insult in muscles of FSHD patients.[8–13] The identification of *DUX4* as a target gene provided a platform to finally enable translational research on FSHD, by allowing the development of *DUX4*-expressing animal models and *DUX4*-targeted molecular therapies.[13–21]

Our laboratory has been working to develop an RNAi-based gene therapy approach to silence the *DUX4* gene as a putative treatment for FSHD.[20] Specifically, we designed single-stranded adeno-associated viral (AAV) vectors carrying U6 promoter-driven artificial microRNAs targeting the *DUX4* mRNA (called miDUX4s). The antisense guide-strands of our miDUX4 constructs contained perfect complementarity with *DUX4* across a 22 nt stretch of sequence, thereby directing the transcript toward an RNAi degradation pathway. In a proof-of-concept study using human cells and mouse muscles overexpressing *DUX4*, we identified a lead sequence, called miDUX4.405 (or mi405), that significantly reduced DUX4 protein and mRNA and improved muscle damage phenotypes associated with large quantities of DUX4 in mice.[20] With an overall goal of translating RNAi therapy for FSHD, in this study our aims were to improve our first-generation miDUX4 vectors, expand the repertoire of sequence options that could be useful for targeting *DUX4*, and safety test our lead sequences in mice and human cells, prior to performing a more expensive good laboratory practice (GLP) toxicology study.
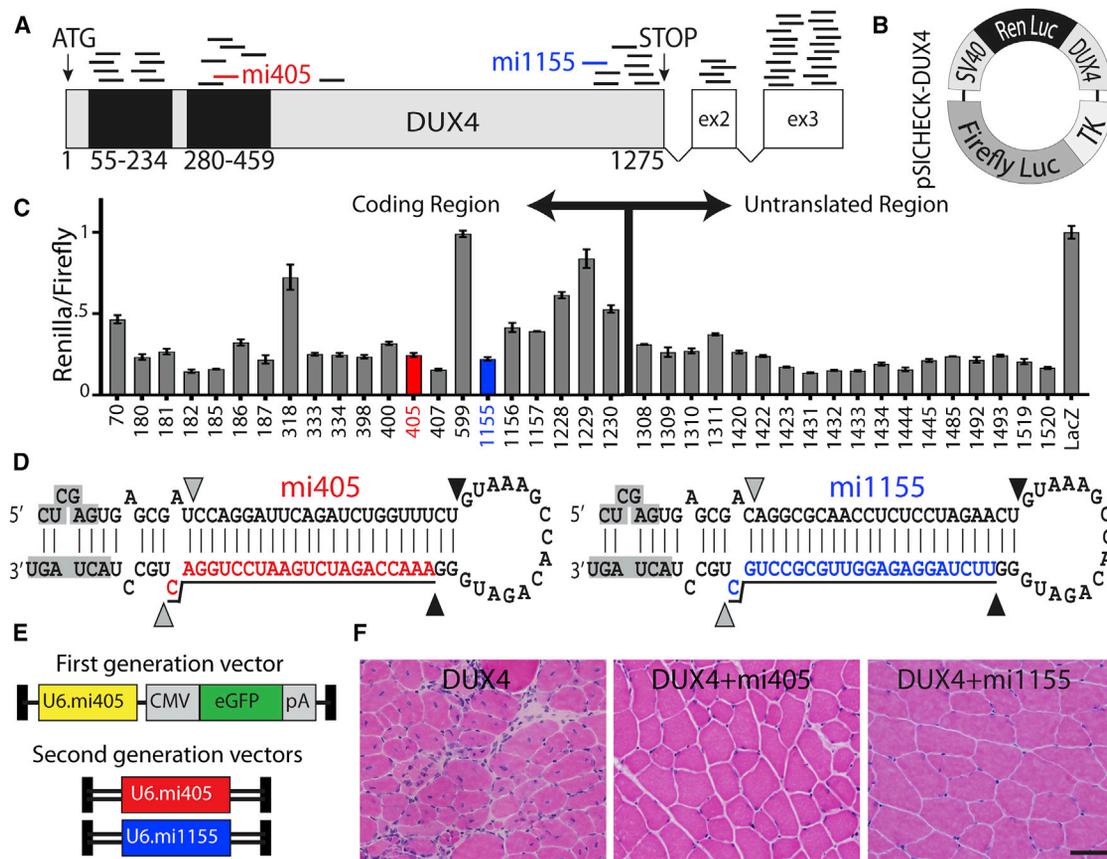
Figure 1. Efficacy Screening and Validation of miDUX4 Sequences

(A) Image represents the *DUX4* transcript, in which exon 1 (shown in gray) contains the entire *DUX4* open reading frame. Black boxes indicate relative positions of ho-meodomain-encoding sequence, provided for orientation. Exons 2 and 3 (ex2 and ex3) encode 3′ UTR regions. The black lines above the *DUX4* transcript represent the relative positions of all miRNAs identified by the Harper lab miRNA shuttle predictor version 1.0. Red and blue lines indicate mi405 and mi1155, the two lead miDUX4s used in the study. Numbers under the schematic correspond to the nucleotide position in the *DUX4* gene, relative to the start codon (ATG). (B) Dual luciferase reporter plasmid used for *in vitro* screening of miDUX4s. The SV40 promoter drives expression of a *Renilla* luciferase (Ren Luc) with *DUX4* cloned as the 3′ UTR. Firefly luciferase is driven by the thymidine kinase promoter (TK) and serves as an internal transfection control. (C) *DUX4* gene silencing was determined by measuring the ratio of *Renilla* to firefly luciferase from HEK293 cells co-transfected with the dual luciferase plasmid and U6-driven miDUX4s expression plasmids. The numbers on the x axis refer to specific miDUX4 sequences (listed in Table S1). Data are displayed as means with error bars representing SD. (D) Hairpin structures and sequences of the two lead miDUX4s in this study, mi405 and mi1155. Gray and black arrowheads indicate Drosha and Dicer cut sites, respectively, while the colored, underlined sequences identify the miRNA guide-strand. Shaded nucleotides are restriction sites used to clone each miRNA into the U6 expression plasmid. (E) Our first-generation single-stranded adeno-associated viral (AAV) vector contained a U6 promoter-driven miDUX4 and a cytomegalovirus (CMV) promoter transcribing EGFP. The second-generation vectors are self-complementary and do not contain EGFP. Black boxes, AAV inverted terminal repeats; pA, SV40 polyadenylation signal. (F) At 2 weeks, DUX4-expressing muscles (left) show histopathological evidence of degeneration, including myofibers with inflammatory infiltrates, central nuclei, and variable fiber size. Co-injections of AAV.DUX4 and scAAV.mi405 or scAAV.mi1155 vectors (middle and right, respectively) are histologically normal, thereby confirming that scAAV bioactivity is similar to that seen using our previously reported single-stranded vectors. Scale bar, 50 μm.

RESULTS

We previously designed and validated five miRNAs targeting *DUX4*.[20] Among this first batch, miDUX4.405 (mi405) performed the best and became our lead sequence. However, as RNAi-based gene therapy is still an emerging field with limited safety data, we wanted to ensure that we had backup sequences that could also be translated toward clinical application in the event of unforeseen mi405 toxicity.[22–24] With that goal in mind, we developed a simple algorithm to select additional miDUX4 sequences. New miDUX4s were designed using the following criteria: 22 nt mature miRNA length, perfect antisense complementarity to the human *DUX4* mRNA, <60% GC content of the mature duplex, and guide-strand biasing, such that the last 4 nucleotides of the antisense 5′ end were A:U rich, and the last 4 nucleotides of the antisense 3′ end were G:C rich. Filtering the *DUX4* gene using these criteria produced 34 new candidates, for a total of 39 miDUX4 sequences tested overall (Figure 1A; Table S1). We cloned each new sequence into a U6 expression plasmid and then performed *in vitro* gene silencing screens in HEK293 cells using a dual luciferase assay in which the *DUX4* cDNA was cloned as the 3′ UTR of *Renilla* luciferase, and

Table 1. AAV Vector Doses, Routes of Administration, and Time Points Used in This Study

Total Particles	vg/kg	Time Point
Intramuscular Delivery[a]		
2×10^{10}	8.5×10^{14}	2 weeks, 8 weeks
1×10^{11}	4.6×10^{15}	2 weeks, 8 weeks
5×10^{11}	2.0×10^{16}	2 weeks, 8 weeks
1.5×10^{12}	6.5×10^{16}	2 weeks, 8 weeks
Intravascular Delivery (ILP)[b]		
3×10^{10}	1.6×10^{12}	3 weeks, 5 months
1×10^{11}	5.6×10^{12}	3, 6, 12 weeks; 5 months
1.5×10^{12}	8.0×10^{13}	3 weeks, 5 months

[a]Vector genomes per kilogram of muscle weight.
[b]Vector genomes per kilogram of body weight.

firefly luciferase was used as a non-targeted transfection control (Figures 1B and 1C).[25] To confirm that silencing of *DUX4* mRNA also reduced overexpressed DUX4 protein, we performed western blots from HEK293 cell protein extracts co-transfected with a V5-epitope-tagged CMV.DUX4 expression plasmid and our individual U6.miDUX4s (Figure S1). Including mi405, we identified 11 miDUX4s (28% of all tested) with >75% silencing using both metrics (mi182, mi185, mi187, mi333, mi334, mi405, mi407, mi1155, mi1434, mi1445, and mi1520). Of these, for practical reasons (time and funding) we selected 2 as our leads (mi1155 and mi405) for further *in vivo* testing in this study, with the additional miDUX4s being tested in ongoing work or reserved as backups until we can feasibly test them (Figure 1D). We noted that roughly three-quarters of our miDUX4 sequences produced >50% DUX4 silencing using *in vitro* assays, thereby validating our miRNA design strategy.

Historically, the template for performing pre-clinical gene therapy studies involved first demonstrating efficacy for a given strategy in disease animal models, followed later by dose escalation safety testing in wild-type animals. Indeed, we began this work several years ago using a similar strategy, by demonstrating proof of principle for the efficacy of RNAi therapy for FSHD targeting *DUX4* in mice.[20] Using a first-generation AAV vector system, we showed that the U6.mi405 sequence could suppress *DUX4* in mouse muscles and prevent toxic outcomes.[20] The first system we published used single-stranded AAV genomes and contained a CMV.EGFP reporter to track transduction; it cannot be translated to human gene therapy (Figure 1E). With an eye toward translation, we generated a second generation of AAV6 vectors, in which we switched to a self-complementary AAV backbone, removed the EGFP reporter, and expressed only the U6 promoter-driven mi405 or mi115 sequences (Figures 1D and 1E). Because our ultimate goal was translation, and because our prior work showed that RNAi-mediated *DUX4* suppression could be efficacious, in this study we decided to depart from the traditional template for translating gene therapy studies and focus primarily on safety outcomes first, prior to performing extensive efficacy studies of

our new vectors and sequences *in vivo*. Thus, we only performed a small bioactivity study to ensure that our second-generation miRNA vectors were suppressing *DUX4*-associated toxicity *in vivo*. To do this, we used our previously published AAV-based DUX4 mouse model (AAV.CMV.DUX4), which shows histological evidence of muscle damage that is useful as an outcome measure for efficacy. Muscles injected with AAV.CMV.DUX4 showed histopathology, while those co-injected with AAV.CMV.DUX4 and scAAV6.mi405 or scAAV6.mi1155 vectors were histologically normal, indicating that our vectors produced the expected bioactivity (n = 6 per group) (Figures 1F and S2).

Previous pre-clinical studies suggested that vector-expressed RNAi triggers such as short hairpin RNAs (shRNAs) could potentially cause adverse effects by two mechanisms: overexpression-related toxicity through saturation of the natural microRNA biogenesis pathway and unintended sequence-specific silencing of off-target genes.[23,24,26,27] We therefore investigated the safety of our lead miDUX4 sequences on the basis of these two potential mechanisms. To address potential adverse events associated with inhibitory RNA overexpression, we first performed dose escalation of scAAV6.mi1155 or scAAV6.mi405 in wild-type mice using intramuscular (i.m.) and intravascular (i.v.) routes of administration (Table 1; Figures 2, 3, and S3). For i.m. injection, we delivered four different doses of scAAV vectors and assessed muscle histology 2 and 8 weeks later. For a vascular approach, we delivered three doses using isolated limb perfusion (ILP) and performed necropsy on tibialis anterior (TA) muscle, diaphragm, lung, liver, spleen, kidney, gonads, and heart at 3 week, 6 week, 12 week, and 5 month time points.[28,29] TA muscles were analyzed using independent blinded analysis by a neuromuscular histopathologist, while independent veterinary pathologists at The Ohio State University Comparative Animal and Mouse Phenotyping Shared Resource assessed other tissues.

Using both delivery methods, we found histological evidence for dose-dependent muscle toxicity in scAAV.mi1155-treated animals (Figure 2). In particular, escalating i.m. vector doses caused increased amounts of regenerated myofibers (indicated by centrally located myonuclei in H&E-stained cryosections), demonstrating that muscles had been damaged and were subsequently repaired in the 8 weeks prior to this time point (Figure 2A). Lower, clinically relevant doses appeared normal (2×10^{10} particles) to relatively normal (1×10^{11} particles) histologically at this time point. Artificially shaded areas (purple) on whole-muscle composite images show the extent of muscle regeneration (Figure 2A). Similar to our i.m. results, animals that received low-dose (3×10^{10} particles) scAAV.mi1155 via ILP injection showed no overt histological evidence of muscle damage at either time point (Figure 2B). Interestingly, muscle injected with high-dose scAAV.mi1155 (1.5×10^{12} particles) appeared normal at 3 weeks but showed widespread regeneration by 5 months, indicating a temporal component to mi1155 toxicity. Besides muscle, mi1155-treated mice showed cellular infiltrates with occasional hepatocellular single-cell necrosis in the liver, but this finding was also present in the controls and considered part of the strain background. Otherwise, no
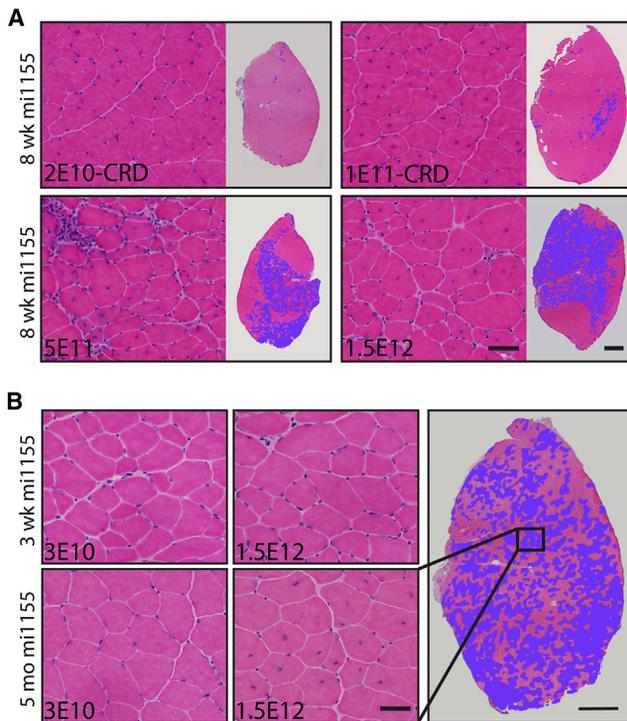
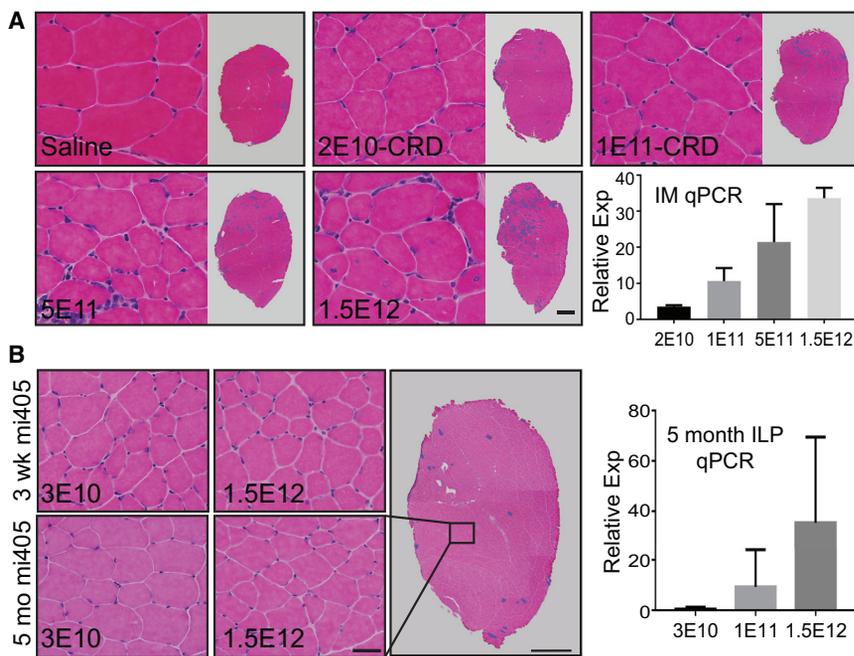**Figure 2. In Vivo Dose Escalation of scAAV.mi1155 in Wild-Type Mice**

(A) Photomicrographs of adult mouse tibialis anterior (TA) muscles 8 weeks after intramuscular (i.m.) injection with the indicated doses of vector. Images show 10 μm cryosections stained with H&E at high and low power. To help visualize the breadth of potential lesions on low-power images, fibers with central nuclei (CN) or areas of active degeneration and inflammation were intentionally shaded with a purple digital overlay. Lesion size correlates with increasing doses of scAAV.mi1155. High-power photos show representative images at indicated vector dosages. CRD indicates a clinically relevant dose range used in previous muscle gene therapy clinical trials. (B) Photomicrographs of adult mouse TA muscles 3 weeks (top) or 5 months (bottom) after vascular delivery of scAAV.mi1155, with the indicated doses of vector. Myofibers with central nuclei, indicating muscle damage and regeneration, were abundant in the 5-month high-dose muscles, as seen in the bottom-right high-power image and visualized in the purple overlay areas of the low-powered photomicrograph. Scale bars, 50 μm for high-power; 500 μm for low-power images.

obvious organ pathology was observed in any of the scAAV.mi1155-treated animals (Supplemental Results; Table S2).

In contrast to the mi1155 sequence, scAAV.mi405 was generally well tolerated following either route of administration. At clinically relevant i.m. doses, mi405-treated muscles were histologically normal relative to saline-injected muscles (Figure 3A). We did note a comparatively larger area of mouse TA muscle with central nuclei at the two highest doses, but even these levels were relatively safe compared with the damage seen in mi1155-treated muscles, and we note that the amount of vector we delivered in the two high-dose groups has never been injected in humans i.m. Muscles treated with mi405 using i.v. delivery appeared histologically indistinguishable from saline-treated muscles, regardless of dose or time point (Figure 3B). Because the

scAAV.mi405-treated muscles showed little to no pathology, we wanted to ensure that the vector was expressing mi405 as expected and therefore developed an adaptor-based TaqMan assay to detect the mature mi405 sequence in vivo. Importantly, mi405 was detected in all treated muscles, and its expression increased with increasing scAAV.mi405 doses, by both i.m. and ILP delivery routes (Figure 3). As was the case for mi1155-treated animals, mi405-treated mice also showed cellular infiltrates with occasional hepatocellular single-cell necrosis in the liver, but this finding was also present in the controls and considered part of the strain background. Otherwise, no obvious organ pathology was observed in any of the scAAV.mi405-treated animals (Supplemental Results).

We next addressed the potential of mi405 or mi1155 to cause unintended, sequence-specific silencing of non-target genes (i.e., sequence-specific off-target effects). We are interested in translating this potential gene therapy approach to human muscles, so we performed this experiment in human muscle cell lines. To do this, we transfected normal, DUX4-negative human myoblasts with AAV proviral plasmids expressing mi405, mi1155, or a control plasmid and then performed RNA sequencing (RNA-seq) to assess gene expression changes. Surprisingly few genes were significantly changed, with only five and seven transcripts reduced >2-fold in mi1155- and mi405-treated cells, respectively (Table 2). Interestingly, three transcripts (PDGFRL, LAMP3, and C1QTNF1) were changed in response to both miDUX4s, despite the fact that mi405 and mi1155 bind completely different regions of the DUX4 transcript and have different seed matches. This suggested their downregulation did not occur through a sequence-specific mechanism. Nevertheless, we queried the sequences of each downregulated transcript identified by RNA-seq against our mi405 and/or mi1155 guide and passenger strands using two different algorithms, siSPOTR and PITA, to identify potential seed match binding sites.[26,30–32] Using this analysis, three transcripts had potential seed matches with mi1155, while two had predicted seeds for mi405 (Table 2). To determine if these potential sites were capable of mediating strong binding between a target transcript and the mi405 or mi1155 sequences, we developed a molecular beacon-binding assay (Figure 4A; Table S3). We first determined the binding affinity of mi1155 and mi405 to their respective perfect target sites on DUX4 (mi1155 dissociation constant [K_d] = 0.28 μM; mi405 K_d = 0.65 μM), with mi1155 having a higher binding affinity than mi405. We then performed the identical assay using oligonucleotides representing putative seed matches identified by the PITA algorithm.[30,32] None of the predicted off-target sites showed significant binding affinity with either strand of mi1155 or mi405 in this assay (Figures 4B and S4). Interestingly, the PITA algorithm identified a second putative mi405 binding site within the DUX4 coding region (mi405 On-TS2). The second location had three mismatches with mi405 at the DNA level but only one at the RNA level, because of G:U base pairing occurring in the latter.[33] Using our molecular beacon assay to assess binding of both sequences, we found strong mi405 binding with the mi405 On-TS2 RNA sequence mimic containing a single mismatch (mi405 On-TS2 K_d = 1.20 μM) but no binding with the three-mismatch DNA sequence.

Figure 3. _In Vivo_ Dose Escalation of scAAV.mi405 in Wild-Type Mice

(A) Photomicrographs of adult mouse tibialis anterior (TA) muscles 8 weeks after intramuscular (i.m.) injection with the indicated doses of scAAV.mi405 vector. Images show 10 μm cryosections stained with H&E at high and low power. To help visualize the breadth of potential lesions on low-power images, fibers with central nuclei (CN) or areas of active degeneration and inflammation were intentionally shaded with a purple digital overlay. High-power photos show representative images at indicated vector dosages. CRD indicates a clinically relevant dose range used in previous muscle gene therapy clinical trials. Histologically, all scAAV.mi405-treated muscles, except the highest dose (1.5×10^{12} particles, bottom middle), were similar to saline injected controls (top left). qPCR detection of mature mi405 transcript (bottom right) indicated increasing mi405 expression with vector dose escalation. (B) TA muscles of adult mice were histologically normal 3 weeks and 5 months after vascular delivery of scAAV.mi405, with the indicated doses of vector. The mi405 transcript increased with dose, as detected by qPCR analysis (right). Scale bars, 50 μm for high-power; 500 μm for low-power images. Data are displayed as means with error bars representing SD.

DISCUSSION

The discovery of RNAi ushered in a new era of molecular biology and expanded the field of gene therapy to include gene-silencing strategies for dominant genetic diseases and viral pathogenesis.[20,34–43] Perhaps not surprisingly, there was early enthusiasm about RNAi as a potentially revolutionary molecular therapy, followed by the realization that developing new technologies into market-ready treatments is typically not an overnight venture. Today, 16 years after RNAi was first described in mammalian cells, RNAi-based treatments are still experimental, although the first RNAi-based commercial products using oligonucleotides are on the near horizon.[44–48] In contrast to oligonucleotide RNAi drugs, RNAi-based gene therapies using AAV vectors are still emerging, and most are still in pre-clinical stages.[20,34,36,38,39,43] ClinicalTrials.gov lists only two clinical trials to date that were designed to test the safety of delivering inhibitory RNAs from AAV vectors in human beings, and both were targeting hepatitis viruses in the liver (ClinicalTrials.gov identifiers NCT01899092 and NCT02315638).[40,49,50] Importantly, no adverse events have been reported, and although they represent an excellent start for the RNAi gene therapy field, safety data regarding long-term expression of inhibitory RNAs from AAV vectors remains limited. For this reason, we focused primarily on safety here, before performing an extensive pre-clinical efficacy assessment using our second-generation vectors (Figure 1).

In this study, we were interested in further developing a gene therapy approach to target the _DUX4_ gene using AAV and RNAi, as a prospective treatment for the dominant muscle disease FSHD. Our major aim here was to identify our lead _DUX4_-targeted miRNA sequences (called miDUX4s) and test the safety of our system with respect to

miDUX4 overexpression in mammalian muscle (our target tissue for this therapy) and the potential reduction of non-_DUX4_, off-target genes in human muscle cell lines. Because mice and humans have homologous miRNA biogenesis and gene-silencing machinery, mouse models are useful for testing the safety impacts of miDUX4 overexpression in muscle. However, for the sequence-specific off-targeting experiment, we tested the potential off-target impacts of miDUX4 sequences in human cells because we ultimately want to apply this system to human gene therapy, and mice and humans have different transcriptomes. Of the two sequences we safety-tested, mi1155 was overtly toxic to muscle, whereas mi405 was not when delivered at clinically relevant doses. The fact that the low-dose mi1155 sequences were well tolerated at early time points but eventually caused whole-scale muscle turnover suggested that the toxic effects were related to accumulation of the mi1155 product over time. We are uncertain about a mechanism to explain this differential toxicity between mi1155 and mi405 on the basis of our current data. Both miRNAs were generated using identical design rules, each was expressed from the identical U6 promoter cloned into the same site within the same AAV vector system, and each was delivered to inbred C57BL/6 mice using identical routes of administration. Expressing either sequence in human cells caused surprisingly few gene expression changes, and the few transcripts that showed significant changes were reduced only 2-fold and did not seem to be targets of either strand of the mature mi405 or mi1155 sequence on the basis of our molecular beacon-binding assays (Figure 4; Table 2). Because we did not measure the impacts of mi1155 on mouse-specific transcripts, it is possible that the mi1155 sequence caused significant off-target reduction of a transcript required for healthy mouse muscle _in vivo_ and that this hypothetical off-target silencing could have contributed

Table 2. RNA-Seq Gene Expression Changes in Human Myoblasts Expressing mi405 or mi1155

			Predicted Off-Target Silencing			
			Guide-Strand		Passenger Strand	
Symbol	Fold Change	p Value	siSPOTR	PITA	siSPOTR	PITA
mi1155						
PDGFRL	−2.29	8.2e-05	–	–	–	–
BIRC3	−2.16	1.4e-06	–	–	–	–
LAMP3	−2.11	1.6e-04	yes	yes	yes	yes
CIQTNF1	−2.11	1.6e-04	–	yes	–	–
GPB4	−2.00	9.7e-06	yes	yes	–	–
mi405						
CXCL11	−2.61	1.2e-05	yes	yes	–	–
LAMP3	−2.46	1.2e-05	–	–	–	–
PDGFRL	−2.42	3.5e-05	–	–	–	–
SERPINA3	−2.13	1.9e-03	–	–	–	–
CIQTNF1	−2.04	1.9e-03	yes	yes	yes	yes
LOC105375913	−2.03	6.0e-03	–	–	–	–
IL32	−2.02	7.2e-03	–	–	–	–

to the muscle damage evident in mi1155-treated animals. However, because the mi405 sequence was non-toxic at clinically relevant doses and showed no significant off-targeting in human muscle cells, we decided to simply discard the mi1155 sequence for future use and focus on translating the mi405 sequence. In addition, in the future we will perform similar safety studies for other high-performing miDUX4 sequences (Figures 1 and S1).

Because of the limited safety profile of RNAi-based gene therapy vectors and the difficulty to predict which sequences will be tolerated well and which will not, we propose that our results underscore the importance of performing a toxicology screen at early pre-clinical stages, using research-grade vectors produced under non-GLP conditions. Lead candidates that pass this initial safety test can then proceed to investigational new drug (IND)-enabling toxicology assessments in mice and perhaps larger animal models, as well as scaled for production in a good manufacturing practice (GMP) vector-manufacturing facility. We believe that this strategy will ultimately save time and money as we and others work to translate RNAi-based gene therapies toward clinical application. Toward this end, we could envision the first FSHD-directed AAV-RNAi clinical trial involving direct i.m. injection to a single muscle or potentially using a vascular approach, because more gene therapy studies are moving toward this route of delivery. Other issues that need to be addressed include establishment of the AAV serotype to use for miDUX4 delivery, inclusion and exclusion criteria for patient recruitment, defining outcome measures, and of course clinical vector production issues. As we begin approaching this milestone, it will be critical to engage with regulatory bodies and clinical experts in FSHD and neuromuscular disease gene therapy to design a prospective future trial involving AAV-delivered mi405, as

well as other lead candidates that emerge through the pipeline we are establishing here.

MATERIALS AND METHODS

### Sequence Generation and Cloning of miDUXs

The Harper miRNA shuttle predictor version 1.0 was created and written in Java, enabling use of the application on Mac OS X and Windows machines. In the application, the user inputs the DNA sequence of a gene of interest, allowing the program to systematically look at 22 characters in a row beginning with the first input nucleotide and subsequently screening the entire sequence moving one character at a time. A potential 22 nt miRNA must meet three criteria to be included in the output file: (1) the first four characters must be at least 75% G and C, (2) the last four characters must be at least 75% A and U, and (3) the entire string of characters must be at least 40% A and U. The output file is a compilation of all these sequences in text file format. For *DUX4*, the predictor identified 44 new candidate miDUX4s (Table S1). All miDUX4s were cloned into the mir-30-based/U6 construct, as previously described.[20] Ten miDUX4s were removed from analysis because of binding disruption from the V5 tag (mi1253, mi1254, and mi1267) or excluded sequence from the 3′ UTR (mi1552, mi1553, mi1554, mi1555, mi1557, mi1558, and mi1559). This program does not exclude sequences containing a run of four or more T nucleotides. Such sequences would be problematic if using a U6 or other RNA pol III promoter, which uses a terminator signal of four or five T's. However, RNA pol II promoters could express miRNAs containing these poly-T regions.

Luciferase Assay

The dual luciferase reporter plasmid was modified from Psicheck2 (Promega) with a firefly luciferase cassette serving as a transfection control and the human *DUX4* gene (coding region plus 3′ UTR including introns) cloned downstream of the *Renilla* luciferase stop codon, serving as a 3′ UTR. HEK293 cells were co-transfected (Lipofectamine 2000; Invitrogen) with the luciferase *DUX4* reporter and individual U6.microRNA expression plasmids in a 1:5 molar ratio. *DUX4* gene silencing was determined as previously described.[20] Triplicate data were averaged per experiment and individual experiments performed two to four times. Results were reported as the average ratio of *Renilla* to firefly luciferase activity ± SD for all combined experiments.

Western Blots

HEK293 cells were co-transfected (Lipofectamine 2000) with a CMV.DUX4.V5 expression vector containing the *DUX4* 3′ UTR and U6.miDUX4s or control U6.miLacZ in a 1:5 molar ratio. Protein was extracted in M-PER Mammalian Protein Extraction Reagent (Thermo Fisher Scientific) 24 hr later and quantified using the DC Protein Assay (Bio-Rad). Fifteen microgram samples were separated on 12% SDS-PAGE, transferred to nitrocellulose membrane, and incubated with the following antibodies: mouse monoclonal antibody to V5 (horseradish peroxidase [HRP]-coupled) (1:5,000, R961-25; Invitrogen); mouse monoclonal GAPDH antibody (1:1,000, CB1001; Millipore), or goat polyclonal GAPDH (1:500, ab9483;
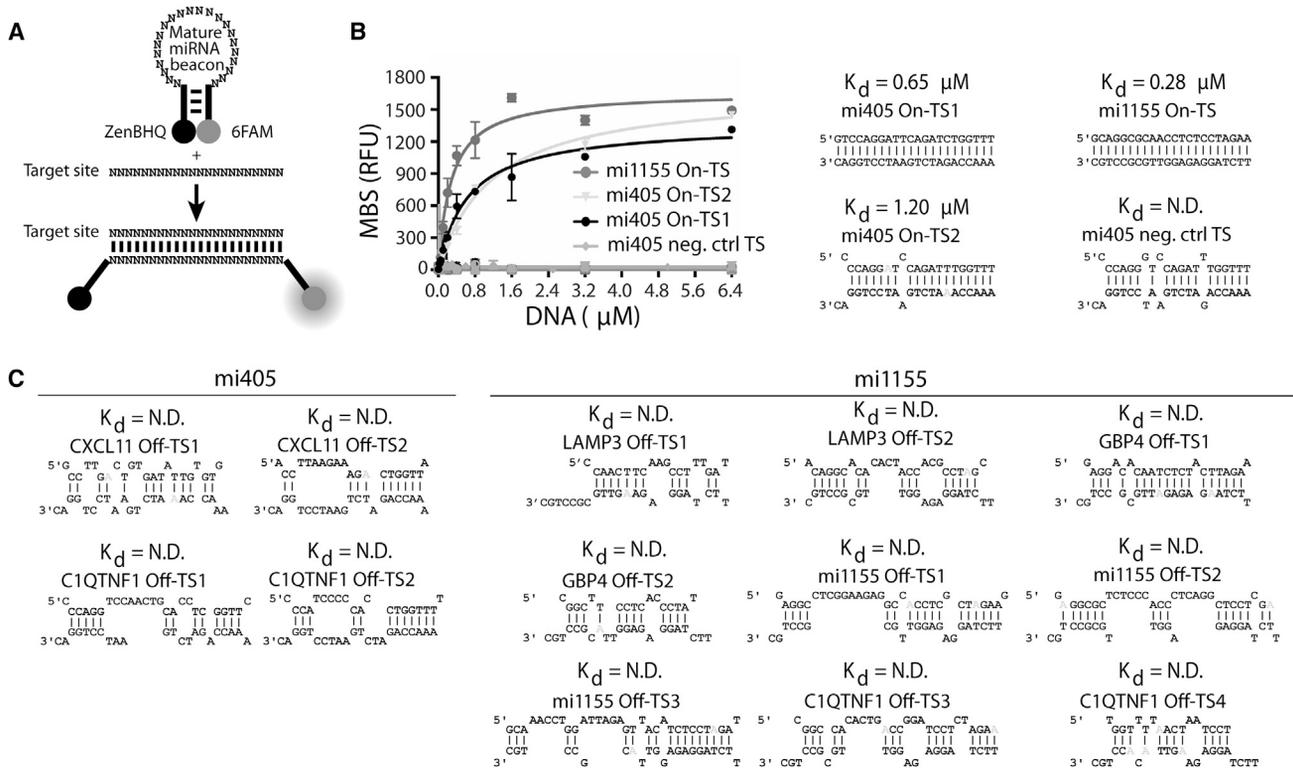
Figure 4. mi405 and mi1155 Bind Specifically to Cognate Target Sites but Not Off-Target Sites

(A) A fluorescence-based molecular beacon assay was used to determine mi405 and mi1155 binding to DUX4 sequences and putative off-targets. By default, the molecular beacon folds into a stem loop structure that brings a quencher (zenBHQ) in close proximity to a fluorophore (6FAM), thereby quenching the fluorescence emission of 6FAM. We designed molecular beacons encompassing the mature sequences of mi405 and mi1155 in their loop sequence. The hybridization of the molecular beacon to a complementary sequence (represented here by a target site) separates the fluorophore and quencher, allowing fluorescence emission. The binding of a mature miRNA beacon to its target site can then be determined by measuring the emitted fluorescence. (B) The graph shows binding data for mi405 and mi1155 target sites within the *DUX4* transcript, where mi405 bound two target sites (mi405 On-TS1 and mi405 On-TS2). The latter had a single mismatch within the 22 nt duplex and two terminal mismatches. mi1155 had strongest binding to its on-target site within *DUX4* ($K_d = 0.28 \mu M$). The mi405 mature sequence bound its perfect target (mi405 On-TS1) with a K_d of 0.65 μM, with reduced binding at the second site (mi405 On-TS2; $K_d = 1.20 \mu M$). A negative control containing two additional mismatches within the mi405 On-TS2 duplex did not bind the mi405 molecular beacon (mi405 neg. ctrl TS). The molecular beacon signal expressed in relative fluorescence units (RFU) was subtracted from background fluorescent signal and used to determine the binding affinity (K_d), which is the binding site concentration (μM) required to reach half of maximum fluorescence. Data are displayed as means with error bars representing SD. (C) Putative off-target sites for mi405 and mi1155 in the indicated transcripts, as determined by PITA analysis of transcripts (*CXCL11*, *C1QTNF1*, *LAMP3*, and *GBP4*) that were significantly reduced in *DUX4*-negative human myoblasts expressing mi405 or mi1155 (specific sites are listed in Materials and Methods). The mi405 and mi1155 molecular beacons showed no binding affinity to any putative off-target sites. For cost and efficiency, the molecular beacon-binding assay was performed using DNA oligonucleotides. To mimic G:U base pairing that occurs in RNA:RNA duplexes, we generated RNA "mimic" bases in the miRNA:off-target site pair, such that A:T base pairing (pairing with two hydrogen bonds) was introduced, replacing the "G" nucleotide with an "A" nucleotide whenever the "G" is facing a "T." These changes are indicated by gray-shaded nucleotides. miRNA:off-target site pairs are represented as two annealing strands. The top strand represents the target site, and the bottom strand represents the mature miDUX4 sequence.

Abcam) overnight at 4°C. GAPDH-probed blots were washed and then incubated with HRP-coupled goat anti-mouse or HRP-coupled donkey anti-goat secondary antibody (1:100,000, 115-035-003 and 705-035-147; Jackson ImmunoResearch) for 1 hr at room temperature. Following washes, blots were developed using Immobilon Western HRP substrate (Millipore) and exposed to film. DUX4.V5 quantification was assessed using ImageJ.

AAV Vector Delivery to Mice

For the bioactivity and i.m. dose escalation studies, 6- to 9-week-old C57BL/6 male and female mice received direct 40 μL i.m. injections into the TA. Bioactivity mice received adeno-associated virus AAV6.CMV.DUX4.V5 at 3×10^9 DNase-resistant particles (DRP) and a contralateral co-injection of AAV6.CMV.DUX4.V5 at 3×10^9 and either scAAV6.U6.mi405 or scAAV6.U6.mi1155 at 3×10^{10} and 1×10^{11} DRP. Muscles were harvested 2 weeks post-injection. N = 6 mice per vector. I.m. dose escalation mice received either saline control or scAAV6.U6.mi405 or scAAV6.U6.mi1155 at 2×10^{10}, 1×10^{11}, 5×10^{11}, or 1.5×10^{12} DRP. Injections were delivered bilaterally and harvested 2 or 8 weeks post-injection. N = 6 legs per dose per time point. For vascular delivery, ILPs were performed on 5- to 6-week-old C57BL/6 male mice as previously described.[28]

Saline injections served as the controls, and AAV6.U6.mi405 or 1155 vectors were delivered at 3×10^{10}, 1×10^{11}, or 1.5×10^{12} DRP. Mice were harvested at 3 weeks post-injection (n = 2 per dose per treatment), 6 and 12 weeks post-injection (n = 3 at 1×10^{11} DRP per treatment), and 5 months post-injection (n = 5 per dose per treatment). All mouse procedures were performed following guidelines approved by the Institutional Animal Care and Use Committee (IACUC) at the Research Institute at Nationwide Children's Hospital.

Histology and Comparative Pathology
Dissected TA muscles were placed in O.C.T. Compound (Tissue-Tek) and frozen on liquid nitrogen-cooled isopentane. Cryosections were cut at 10 μm and then stained with H&E following standard protocols.[51] Dissected diaphragm, kidney, liver, heart, spleen, testis, and lung (needle perfused) were all post-fixed in 10% neutral buffered formalin for 48 hr and then processed, paraffin-embedded, cut, and H&E-stained at the Nationwide Children's Hospital Morphology Core Laboratory. TA muscles were analyzed by a blinded neuropathologist, and all other tissues were analyzed at The Ohio State University Comparative Pathology & Mouse Phenotyping Shared Resource.

mi405 qPCR Assay
The mi405 qPCR protocol was designed on the basis of methods previously described.[52] Briefly, RNA was extracted using the total RNA protocol for the mirVana miRNA Isolation Kit (Ambion) from 25 50 μm cryosections of indicated TA muscles. cDNA was generated using the High-Capacity cDNA Reverse Transcription Kit (Applied Biosystems) using a mix of random hexamer primers and 200 nM of the stem-loop forming primer (5′-GTC GTATCCAGTGCAGGGTCCGAGGTATTCGCACTGGATACGA CGTCCAG-3′). A custom TaqMan assay (Applied Biosystems) including 1.5 μM of forward primer (5′-CGGCCCAAACCAGATCT GAATC-3′), 0.7 μM of reverse primer (5′-GTGCAGGGTCCGA GGT-3′), and 0.2 μM of mi405 probe (5′-6FAM-ATACGACGTCC AGGAT-3′) was then run using the CFX Connect Real Time system apparatus (Bio-Rad). *RPL13* (Mm02526700_g1; Applied Biosystems) served as the reference gene, and normalized expression (ΔΔCq) was calculated relative to the lowest viral dose per experiment (2×10^{10} DRP for i.m. and 3×10^{10} DRP for ILP).

RNA-Seq and Off-Target Analysis
Human immortalized myoblasts were transfected with an AAV proviral plasmid expressing U6.mi405, U6.1155, or control plasmid pCINeo using the Human Dermal Fibroblast Nucleofector kit (Amaxa). RNA preparation, library construction, quality control, and sequencing were performed as previously described.[53] pCINeo controls were previously described as simultaneous experiments were run together using the same control group.[53] Gene expression changes with fold change of ±2.00 and p values < 0.05 compared with controls were considered significant. These genes were then analyzed for miDUX4 seed matching, and the predicted identity of all off-target sites in every off-target gene using two different prediction programs: siSPOTR and the PITA prediction algorithm.[27,30]

RNA-seq was performed by The Biomedical Genomics Core of the Research Institute at Nationwide Children's Hospital, Columbus, Ohio. Raw data files for the RNA-seq data are deposited at https://www.ncbi.nlm.nih.gov/sra/SRP127959 (SRA: SRP127959).

Molecular Beacon-Binding Assay
Mature DNA sequences of mi405 and mi1155 complementary to their cognate target sites were designed and used as previously described.[54] A 6FAM fluorophore and a Zen Black Hole Quencher (ZenBHQ) were added at the 5′ and 3′ ends, respectively. The DNA molecular beacons were synthesized (Integrated DNA Technologies), and each molecular beacon had a density close to 3 OD and was purified using high-performance liquid chromatography (HPLC). The binding assay was performed as previously described, with some modifications.[54] The binding assay was performed using the CFX Connect Real Time system apparatus. After mixing the molecular beacon and target site, the binding was initiated with a denaturation step at 95°C for 3 min, followed by an annealing step at 37°C for 10 min. The fluorescence was measured at the end of the annealing step.

The relative fluorescent signal (relative fluorescence units [RFU]) was subtracted from background fluorescent signal and fit to a one site-specific binding Hill slope equation that was used to determine the binding affinity (K_d). The mi405 and mi1155 molecular beacons were used at a constant concentration of 200 nM, and the constant parameter (K_d) was determined by increasing the concentration of the cognate target sites. K_d is the binding site concentration (nM) required to reach half of the maximum fluorescence and represents binding affinity. The smaller the K_d value, the greater the binding affinity of the miRNA molecular beacon is for its target site. We tested binding of off-target genes identified by RNA-seq (Table 2) and queried PITA and siSPOTR to identify transcripts with putative binding sites for mi405 and mi1155. We modified our molecular beacon assay by using DNA oligos designed to mimic G:U base pairing (two hydrogen bonds) that occurs in RNA:RNA duplexes. To mimic RNA:RNA base pairing in the miRNA:off-target site pair, A:T base pairing (pairing with two hydrogen bonds) was introduced, replacing the "G" nucleotide with an "A" nucleotide whenever the "G" is facing a "T."

Predicted target sites are indicated as follows. mi405 On-TS1: on-target site on *DUX4* open reading frame (ORF) at position 405; mi405 On-TS2: second on-target site on *DUX4* ORF at position 193; and mi1155 On-TS: on-target site on *DUX4* ORF at position 1155. The remaining annealing strands represent pairing of mi405 or mi1155 to their off-target sites. *CXCL11* Off-TS1: mi405 off-target site on *CXCL11* ORF at position 28; *CXCL11* Off-TS2: mi405 off-target site on *CXCL11* 3′UTR at position 281 from the beginning of 3′ UTR; *C1QTNF1* Off-TS1: mi405 off-target site on *C1QTNF1* ORF at position 21; *C1QTNF1* Off-TS2: mi405 off-target site on *C1QTNF1* 3′ UTR at position 1494 from the beginning of 3′ UTR; *LAMP3* Off-TS1: mi1155 off-target site on *LAMP3* ORF at position 1310; *LAMP3* Off-TS2: mi1155 off-target site on *LAMP3* 3′ UTR at

position 663 from the beginning of 3′UTR; *GBP4* Off-TS1: mi1155 off-target site on *GBP4* ORF at position 1466; *GBP4* Off-TS2: mi1155 off-target site on *GBP4* 3′ UTR at position 3181 from the beginning of 3′ UTR; mi1155 Off-TS1: mi1155 off-target site on *DUX4* ORF at position 1194; mi1155 Off-TS2: mi1155 off-target site on *DUX4* ORF at position 767; mi1155 Off-TS3: mi1155 off-target site on *DUX4* 3′ UTR at position 2050 from the beginning of 3′ UTR; *C1QTNF1* Off-TS3: mi1155 off-target site on *C1QTNF1* ORF at position 19; *C1QTNF1* Off-TS4: mi1155 off-target site on *C1QTNF1* 3′ UTR at position 1495 from the beginning of 3′UTR.

SUPPLEMENTAL INFORMATION
Supplemental Information includes Supplemental Results, four figures, and three tables and can be found with this article online at https://doi.org/10.1016/j.omtm.2017.12.005.

AUTHOR CONTRIBUTIONS
L.M.W. designed and performed all mouse experiments and necropsies (except ILP surgeries), designed and performed qPCR assays, and contributed to western blots, RNA-seq experiments, and analysis. L.M.W. also created figures and legends and wrote the Materials and Methods section of the paper. N.Y.S. designed and performed the molecular beacon assay and created figures, legends, and methods with the assayed data. N.K.P. and J.S.D. cloned and tested the new miDUX4s *in vitro*. N.K.P. generated a supplemental figure and table with *in vitro* data. A.M.F. produced and titered all AAV vectors. J.O.E. contributed to RNA-seq experiments. D.A.G. and L.R.R.-K. performed ILP surgeries and contributed to experimental design. A.C.H. created the algorithm used to identify new candidate miDUX4s. Z.S. was the pathologist who analyzed TA muscle histology. S.Q.H. conceptualized and obtained funding for the project, designed the miRNA predictor criteria, contributed to data analysis, and wrote the manuscript. All authors contributed to refining and editing the manuscript.

REFERENCES
1. Deenen, J.C., Arnts, H., van der Maarel, S.M., Padberg, G.W., Verschuuren, J.J., Bakker, E., Weinreich, S.S., Verbeek, A.L., and van Engelen, B.G. (2014). Population-based incidence and prevalence of facioscapulohumeral dystrophy. Neurology 83, 1056–1059.

2. Flanigan, K.M., Coffeen, C.M., Sexton, L., Stauffer, D., Brunner, S., and Leppert, M.F. (2001). Genetic characterization of a large, historically significant Utah kindred with facioscapulohumeral dystrophy. Neuromuscul. Disord. 11, 525–529.

3. Padberg, G.W. (1982) Facioscapulohumeral disease. PhD thesis (Leiden, the Netherlands: Leiden University).

4. FSH Society (2016) Facts & statistics. https://www.fshsociety.org/facts-statistics/.

5. Statland, J.M., McDermott, M.P., Heatwole, C., Martens, W.B., Pandya, S., van der Kooi, E.L., Kissel, J.T., Wagner, K.R., and Tawil, R. (2013). Reevaluating measures of disease progression in facioscapulohumeral muscular dystrophy. Neuromuscul. Disord. 23, 306–312.

6. Flanigan, K.M., and Harper, S.Q. (2013). Facioscapulohumeral dystrophy. In Muscle Disease, H.H. Goebel, C. Sewry, and R. Weller, eds. (John Wiley & Sons), pp. 288–297.

7. Statland, J.M., and Tawil, R. (2014). Risk of functional impairment in facioscapulohumeral muscular dystrophy. Muscle Nerve 49, 520–527.

8. Bosnakovski, D., Xu, Z., Gang, E.J., Galindo, C.L., Liu, M., Simsek, T., Garner, H.R., Agha-Mohammadi, S., Tassin, A., Coppée, F., et al. (2008). An isogenetic myoblast expression screen identifies DUX4-mediated FSHD-associated molecular pathologies. EMBO J. 27, 2766–2779.

9. Dixit, M., Ansseau, E., Tassin, A., Winokur, S., Shi, R., Qian, H., Sauvage, S., Mattéotti, C., van Acker, A.M., Leo, O., et al. (2007). DUX4, a candidate gene of facioscapulohumeral muscular dystrophy, encodes a transcriptional activator of PITX1. Proc. Natl. Acad. Sci. U S A 104, 18157–18162.

10. Gabriëls, J., Beckers, M.C., Ding, H., De Vriese, A., Plaisance, S., van der Maarel, S.M., Padberg, G.W., Frants, R.R., Hewitt, J.E., Collen, D., and Belayew, A. (1999). Nucleotide sequence of the partially deleted D4Z4 locus in a patient with FSHD identifies a putative gene within each 3.3 kb element. Gene 236, 25–32.

11. Kowaljow, V., Marcowycz, A., Ansseau, E., Conde, C.B., Sauvage, S., Mattéotti, C., Arias, C., Corona, E.D., Nuñez, N.G., Leo, O., et al. (2007). The DUX4 gene at the FSHD1A locus encodes a pro-apoptotic protein. Neuromuscul. Disord. 17, 611–623.

12. Lemmers, R.J., van der Vliet, P.J., Klooster, R., Sacconi, S., Camaño, P., Dauwerse, J.G., Snider, L., Straasheijm, K.R., van Ommen, G.J., Padberg, G.W., et al. (2010). A unifying genetic model for facioscapulohumeral muscular dystrophy. Science 329, 1650–1653.

13. Wallace, L.M., Garwick, S.E., Mei, W., Belayew, A., Coppee, F., Ladner, K.J., Guttridge, D., Yang, J., and Harper, S.Q. (2011). DUX4, a candidate gene for facioscapulohumeral muscular dystrophy, causes p53-dependent myopathy in vivo. Ann. Neurol. 69, 540–552.

14. Chen, J.C.J., King, O.D., Zhang, Y., Clayton, N.P., Spencer, C., Wentworth, B.M., Emerson, C.P., Jr., and Wagner, K.R. (2016). Morpholino-mediated knockdown of DUX4 towards facioscapulohumeral muscular dystrophy therapeutics. Mol. Ther. 24, 1405–1411.

15. Dandapat, A., Bosnakovski, D., Hartweck, L.M., Arpke, R.W., Baltgalvis, K.A., Vang, D., Baik, J., Darabi, R., Perlingeiro, R.C., Hamra, F.K., et al. (2014). Dominant lethal pathologies in male mice engineered to contain an X-linked DUX4 transgene. Cell Rep. 8, 1484–1496.

16. Himeda, C.L., Jones, T.I., and Jones, P.L. (2016). CRISPR/dCas9-mediated transcriptional inhibition ameliorates the epigenetic dysregulation at D4Z4 and represses DUX4-fl in FSH muscular dystrophy. Mol. Ther. 24, 527–535.

17. Jones, T.I., Parilla, M., and Jones, P.L. (2016). Transgenic Drosophila for investigating DUX4 and FRG1, two genes associated with facioscapulohumeral muscular dystrophy (FSHD). PLoS ONE 11, e0150938.

18. Krom, Y.D., Thijssen, P.E., Young, J.M., den Hamer, B., Balog, J., Yao, Z., Maves, L., Snider, L., Knopp, P., Zammit, P.S., et al. (2013). Intrinsic epigenetic regulation of the D4Z4 macrosatellite repeat in a transgenic mouse model for FSHD. PLoS Genet. 9, e1003415.

19. Mitsuhashi, H., Mitsuhashi, S., Lynn-Jones, T., Kawahara, G., and Kunkel, L.M. (2013). Expression of DUX4 in zebrafish development recapitulates facioscapulo-humeral muscular dystrophy. Hum. Mol. Genet. 22, 568–577.

20. Wallace, L.M., Liu, J., Domire, J.S., Garwick-Coppens, S.E., Guckes, S.M., Mendell, J.R., Flanigan, K.M., and Harper, S.Q. (2012). RNA interference inhibits DUX4-induced muscle toxicity in vivo: implications for a targeted FSHD therapy. Mol. Ther. 20, 1417–1423.

21. Wuebbles, R.D., Long, S.W., Hanel, M.L., and Jones, P.L. (2010). Testing the effects of FSHD candidate gene expression in vertebrate muscle development. Int. J. Clin. Exp. Pathol. 3, 386–400.

22. Borel, F., Kay, M.A., and Mueller, C. (2014). Recombinant AAV as a platform for translating the therapeutic potential of RNA interference. Mol. Ther. 22, 692–701.

23. Grimm, D., Streetz, K.L., Jopling, C.L., Storm, T.A., Pandey, K., Davis, C.R., Marion, P., Salazar, F., and Kay, M.A. (2006). Fatality in mice due to oversaturation of cellular microRNA/short hairpin RNA pathways. Nature 441, 537–541.

24. McBride, J.L., Boudreau, R.L., Harper, S.Q., Staber, P.D., Monteys, A.M., Martins, I., Gilmore, B.L., Burstein, H., Peluso, R.W., Polisky, B., et al. (2008). Artificial miRNAs mitigate shRNA-mediated toxicity in the brain: implications for the therapeutic development of RNAi. Proc. Natl. Acad. Sci. U S A 105, 5868–5873.

25. Boudreau, R.L., Garwick-Coppens, S.E., Liu, J., Wallace, L.M., and Harper, S.Q. (2011). Rapid cloning and validation of microRNA shuttle vectors: a practical guide. In RNA Interference Techniques, Vol. 1: Neuromethods, S.Q. Harper, ed. (Humana Press), pp. 19–37.

26. Boudreau, R.L., Spengler, R.M., and Davidson, B.L. (2011). Rational design of thera-peutic siRNAs: minimizing off-targeting potential to improve the safety of RNAi therapy for Huntington's disease. Mol. Ther. 19, 2169–2177.

27. Boudreau, R.L., Spengler, R.M., Hylock, R.H., Kusenda, B.J., Davis, H.A., Eichmann, D.A., and Davidson, B.L. (2013). siSPOTR: a tool for designing highly specific and potent siRNAs for human and mouse. Nucleic Acids Res. 41, e9.

28. Rodino-Klapac, L.R., Janssen, P.M., Montgomery, C.L., Coley, B.D., Chicoine, L.G., Clark, K.R., and Mendell, J.R. (2007). A translational approach for limb vascular delivery of the micro-dystrophin gene without high volume or high pressure for treat-ment of Duchenne muscular dystrophy. J. Transl. Med. 5, 45.

29. Rodino-Klapac, L.R., Montgomery, C.L., Mendell, J.R., and Chicoine, L.G. (2011). AAV-mediated gene therapy to the isolated limb in rhesus macaques. Methods Mol. Biol. 709, 287–298.

30. Kertesz, M., Iovino, N., Unnerstall, U., Gaul, U., and Segal, E. (2007). The role of site accessibility in microRNA target recognition. Nat. Genet. 39, 1278–1284.

31. Davidson Laboratory siSPOTR: siRNA Sequence Probability-of-Off-Targeting Reduction, https://sispotr.icts.uiowa.edu/sispotr/tools/lookup/evaluate.html.

32. Segal Lab of Computational Biology Online microRNA Prediction Tool, https://genie.weizmann.ac.il/pubs/mir07/mir07_prediction.html.

33. Varani, G., and McClain, W.H. (2000). The G x U wobble base pair. A fundamental building block of RNA structure crucial to RNA function in diverse biological systems. EMBO Rep. 1, 18–23.

34. Bisset, D.R., Stepniak-Konieczna, E.A., Zavaljevski, M., Wei, J., Carter, G.T., Weiss, M.D., and Chamberlain, J.R. (2015). Therapeutic impact of systemic AAV-mediated RNA interference in a mouse model of myotonic dystrophy. Hum. Mol. Genet. 24, 4971–4983.

35. Bortolanza, S., Nonis, A., Sanvito, F., Maciotta, S., Sitia, G., Wei, J., Torrente, Y., Di Serio, C., Chamberlain, J.R., and Gabellini, D. (2011). AAV6-mediated systemic shRNA delivery reverses disease in a mouse model of facioscapulohumeral muscular dystrophy. Mol. Ther. 19, 2055–2064.

36. Harper, S.Q., Staber, P.D., He, X., Eliason, S.L., Martins, I.H., Mao, Q., Yang, L., Kotin, R.M., Paulson, H.L., and Davidson, B.L. (2005). RNA interference improves motor and neuropathological abnormalities in a Huntington's disease mouse model. Proc. Natl. Acad. Sci. U S A 102, 5820–5825.

37. Lee, N.S., Dohjima, T., Bauer, G., Li, H., Li, M.J., Ehsani, A., Salvaterra, P., and Rossi, J. (2002). Expression of small interfering RNAs targeted against HIV-1 rev transcripts in human cells. Nat. Biotechnol. 20, 500–505.

38. Liu, J., Wallace, L.M., Garwick-Coppens, S.E., Sloboda, D.D., Davis, C.S., Hakim, C.H., Hauser, M.A., Brooks, S.V., Mendell, J.R., and Harper, S.Q. (2014). RNAi-medi-ated gene silencing of mutant myotilin improves myopathy in LGMD1A mice. Mol. Ther. Nucleic Acids 3, e160.

39. Malerba, A., Klein, P., Bachtarzi, H., Jarmin, S.A., Cordova, G., Ferry, A., Strings, V., Espinoza, M.P., Mamchaoui, K., Blumen, S.C., et al. (2017). PABPN1 gene therapy for oculopharyngeal muscular dystrophy. Nat. Commun. 8, 14848.

40. Suhy, D.A., Kao, S.C., Mao, T., Whiteley, L., Denise, H., Souberbielle, B., Burdick, A.D., Hayes, K., Wright, J.F., Lavender, H., et al. (2012). Safe, long-term hepatic expression of anti-HCV shRNA in a nonhuman primate model. Mol. Ther. 20, 1737–1749.

41. Wallace, L.M., Garwick, S.E., and Harper, S.Q. (2010). RNAi therapy for dominant muscular dystrophies and other myopathies. In Muscle Gene Therapy, D. Duan, ed. (Springer), pp. 99–115.

42. Wallace, L.M., Garwick-Coppens, S.E., Tupler, R., and Harper, S.Q. (2011). RNA interference improves myopathic phenotypes in mice over-expressing FSHD region gene 1 (FRG1). Mol. Ther. 19, 2048–2054.

43. Xia, H., Mao, Q., Eliason, S.L., Harper, S.Q., Martins, I.H., Orr, H.T., Paulson, H.L., Yang, L., Kotin, R.M., and Davidson, B.L. (2004). RNAi suppresses polyglutamine-induced neurodegeneration in a model of spinocerebellar ataxia. Nat. Med. 10, 816–820.

44. Adams, D., Suhr, O.B., Dyck, P.J., Litchy, W.J., Leahy, R.G., Chen, J., Gollob, J., and Coelho, T. (2017). Trial design and rationale for APOLLO, a Phase 3, placebo-controlled study of patisiran in patients with hereditary ATTR amyloidosis with polyneuropathy. BMC Neurol. 17, 181.

45. Davidson, B.L., and McCray, P.B., Jr. (2011). Current prospects for RNA interfer-ence-based therapies. Nat. Rev. Genet. 12, 329–340.

46. Mullard, A. (2016). RNAi hits another rut. Nat. Rev. Drug Discov. 15, 738.

47. Novina, C.D., and Sharp, P.A. (2004). The RNAi revolution. Nature 430, 161–164.

48. Feuerstein, A. (2017). A drug that's part of a brand new class of medicines just got one step closer to approval. Business Insider, September 20, 2017. http://www.businessinsider.com/alnylam-rnai-based-drug-clinical-trial-results-2017-9.

49. Lavender, H., Brady, K., Burden, F., Delpuech-Adams, O., Denise, H., Palmer, A., Perkins, H., Savic, B., Scott, S., Smith-Burchnell, C., et al. (2012). In vitro character-ization of the activity of PF-05095808, a novel biological agent for hepatitis C virus therapy. Antimicrob. Agents Chemother. 56, 1364–1375.

50. Mao, T., et al. (2016). BB-HB-331, a DNA-directed RNA interference (ddRNAi) agent targeting hepatitis B virus (HBV), can effectively suppress HBV in vitro and in vivo. Mol. Ther. 24, S103.

51. Harper, S.Q., Hauser, M.A., DelloRusso, C., Duan, D., Crawford, R.W., Phelps, S.F., Harper, H.A., Robinson, A.S., Engelhardt, J.F., Brooks, S.V., and Chamberlain, J.S. (2002). Modular flexibility of dystrophin: implications for gene therapy of Duchenne muscular dystrophy. Nat. Med. 8, 253–261.

52. Chen, C., Ridzon, D.A., Broomer, A.J., Zhou, Z., Lee, D.H., Nguyen, J.T., Barbisin, M., Xu, N.L., Mahuvakar, V.R., Andersen, M.R., et al. (2005). Real-time quantification of microRNAs by stem-loop RT-PCR. Nucleic Acids Res. 33, e179.

53. Eidahl, J.O., Giesige, C.R., Domire, J.S., Wallace, L.M., Fowler, A.M., Guckes, S.M., Garwick-Coppens, S.E., Labhart, P., and Harper, S.Q. (2016). Mouse Dux is myotoxic and shares partial functional homology with its human paralog DUX4. Hum. Mol. Genet. 25, 4577–4589.

54. Baker, M.B., Bao, G., and Searles, C.D. (2012). In vitro quantification of specific microRNA using molecular beacons. Nucleic Acids Res. 40, e13.